Available online at www.sciencedirect.com
SCIENCE DIRECT®
International Journal of Heat and Mass Transfer 48 (2005) 2571–2581
International Journal of HEAT and MASS TRANSFER
www.elsevier.com/locate/ijhmt

MHD effect on flow structures and heat transfer characteristics of liquid metal–gas annular flow in a vertical pipe

Feng-Chen Li *, Tomoaki Kunugi, Akimi Serizawa

Department of Nuclear Engineering, Kyoto University, Yoshida, Sakyo, Kyoto 606-01, Japan

Received 22 May 2003; received in revised form 19 January 2004
Available online 13 March 2005

Abstract

The magnetohydrodynamic (MHD) effect on the flow structures and heat transfer characteristics was studied numerically for a liquid metal–gas annular flow under a transverse magnetic field. The side layers, in which the velocity was increased, appeared near the eastern and western sidewalls in an annular MHD flow as in a single-phase liquid metal MHD flow. Temperature distribution in the liquid film, and the Nusselt number distribution in the angular direction were influenced by the flow structures with the side layers. Consequently heat transfer rate was higher at the eastern/western sidewalls than that at the southern/northern walls. The pressure drop in the MHD annular flow is of the same order of magnitude as in the single-phase MHD pipe flow under similar liquid metal flow condition.

Keywords: Liquid metal–gas annular flow; MHD effects; Flow structures; Heat transfer; Pressure drop

1. Introduction

The flow of liquid metals in the presence of a magnetic field has been a topic of great interest for several decades. Experimental and mostly analytical studies were performed for the development of magnetohydrodynamic (MHD) devices of electromagnetic flow meters, MHD generators, electromagnetic pumps and accelerators [1–9]. Steady, incompressible rectilinear flow under transverse magnetic field has received most attention of all the areas of MHD flows mentioned above [4,7]. MHD duct flows have been systematically analyzed particularly for the flow in the rectangular duct with both conducting and non-conducting walls.

In recent decades, researches of MHD liquid metal flow have been performed mainly for the development of fusion technology, particularly for the conceptual design of the self-cooled liquid metal blanket of magnetically confined fusion reactor [10], and further for the exploration of innovative concepts for fusion chamber technology, namely, first wall, blanket, divertor and vacuum vessel [11]. A number of experimental and analytical studies have been carried out so far to investigate the hydrodynamic and heat transfer characteristics of the liquid metal flows in a duct and those with free surfaces subjected to MHD forces. Previous studies in this research field have been reviewed by Lielausis [12] and recent understandings have been summarized by Kirillov et al. [13], Morley et al. [14] and Abdou et al. [11].

* Corresponding author. Present address: Second Department, Institute of Industrial Science, The University of Tokyo, De504 4-6-1 Komaba, Meguro-ku, Tokyo 153-8505, Japan. Fax: +81 3 5452 6197.
E-mail address: lifch@icebeer.iis.u-tokyo.ac.jp (F.-C. Li).

0017-9310/$ - see front matter © 2005 Elsevier Ltd. All rights reserved.
doi:10.1016/j.ijheatmasstransfer.2004.12.041

Nomenclature

B_0	magnetic flux density of the uniform field (T)
C_f	friction factor
c_p	specific heat (J/kg K)
g	gravitational acceleration (m/s^2)
Ha	Hartmann number ($Ha = 2B_0R_i\sqrt{\sigma/\mu}$)
h	heat transfer coefficient (W/m^2 K)
j	electric current density (A/m^2)
j_x	electric current density component in the x direction (A/m^2)
j_y	electric current density component in the y direction (A/m^2)
Nu	Nusselt number ($Nu = hR_i/\lambda$)
Nu_{an}	Nusselt number in annular two-phase flow
Nu_{sn}	Nusselt number in single-phase flow
p	pressure (Pa)
q	heat flux (W/m^2)
r	radial coordinate in cylindrical coordinate system
R_0	outer radius of circular pipe (m)
Re	Reynolds number for single-phase flow ($Re = 2\rho V_0R_i/\mu$)
Re_g	gas Reynolds number for annular flow ($Re_g = 2\rho_g V_{0g}R_g/\mu_g$)
Re_L	liquid Reynolds number for annular flow ($Re_L = 2\rho V_{zm}(R_i - R_g)/\mu$)
R_g	radius of gas core (m)
R_i	inner radius of circular pipe (m)
T	temperature (°C)
T_b	bulk temperature (°C)
V	velocity (m/s)
V_0	initial velocity for single-phase flow (m/s)
V_{0g}	average velocity in gas core of annular flow (m/s)
V_z	velocity component in the axial direction (m/s)
V_{zm}	average liquid velocity of annular flow (m/s)
x	x coordinate in Cartesian coordinates (m)
y	y coordinate in Cartesian coordinates (m)
z	axial coordinate in cylindrical coordinate system (m)

Greek symbols

Θ	dimensionless temperature
Θ_b	dimensionless bulk temperature
δ	liquid film thickness of annular flow (m)
ϕ	electric potential (V)
λ	thermal conductivity of liquid (W/m °C)
μ	dynamic viscosity of liquid (Pa s)
μ_g	dynamic viscosity of gas (Pa s)
θ	polar angular coordinate in cylindrical coordinate system
ρ	liquid density (kg/m^3)
ρ_g	gas density (kg/m^3)
σ	electric conductivity of liquid (mho/m)
σ_w	electric conductivity of wall (mho/m)
τ	shear stress (N/m^2).

In the cases of liquid wall concepts for the chamber technology of magnetically confined fusion reactor, the problems emerging from two contradictions have attracted much more attentions. One contradiction is between the efforts to enhance heat transfer rate and to decrease the MHD pressure drop along the flow channel. To enhance heat transfer rate, liquid metals are the best candidates for the working fluids but meanwhile liquid metal flowing in a strong magnetic field inevitably results in excess and actually very serious MHD pressure drop. The other contradiction is between the effort to decrease the MHD pressure drop along the flow channel and the constraints of materials under the operating conditions of a fusion reactor. The non-conducting non-metallic structural devices are the best choice to mitigate magnetic pressure drop due to MHD effects, but non-metallic materials are generally not compatible with liquid metals at high temperature of several hundreds degree centigrade. An idea has been therefore proposed by Bender and Hoffman [15], which uses a gas–liquid metal two-phase flow for the purpose of increasing heat transfer coefficient meanwhile mitigating pressure losses of the flow (since mass flow rate of two-phase flow is less than that of single-phase liquid to remove the same heat flux) and using insulator coatings to degrade the pressure drop. This issue has been intensively investigated [16–20]. Nonetheless, the details of the two-phase MHD flow structure are still worthy to be explored and can be treated preferably by numerical approaches as will be shown later.

It is well known that the MHD flow in a duct can be divided into three regions (as shown in Fig. 2), i.e., core region, the Hartmann layer and side layer [21,22]. The viscous and inertia forces are negligible in the core region where velocity is nearly constant. The shear is so strong that viscous forces can compete with magnetic forces in the Hartmann layer adjoining a solid wall normal to the applied magnetic field. The flow structure in the side layer is strongly dependent on the wall conductance ratio and consequently on the current density distribution. The flow speed in the side layers is higher than

that in other two regions, forming the so-called M-shaped velocity profiles in a MHD duct flow. However, whether or not there are similar flow structures in other situations, e.g., a film flow or open channel flow influenced by the MHD effect has not been investigated.

Serizawa et al. [16] reported, based on their experiment on nitrogen–sodium–potassium eutectic alloy (NaK) annular/annular-dispersed flows, the asymmetric heat transfer characteristics between the wall surfaces parallel to the magnetic field (eastern and western walls, abbreviated as E/W walls hereinafter, as shown in Fig. 2) and those perpendicular to the field direction (northern and southern walls, N/S walls). One of their hypothetical explanations for mechanisms of this phenomenon is the existence of something like side layers in the film flow that could enhance heat transfer at the E/W walls [16,23]. However, the hypothetical velocity profiles have not been verified yet experimentally, since measurement of the velocity distribution in a thin liquid film flow is difficult. The purpose of the present study is then motivated to numerically clarify the flow structures and heat transfer characteristics of the liquid metal–gas annular MHD flows in geometry similar to that used in the experiments [16].

2. Governing equations and procedures

The working liquid is NaK with the mass component of potassium of 78%, and the gas is nitrogen (N_2). The flow channel is a vertical circular stainless steel pipe with inner diameter of 15.75 mm and wall thickness of 1.65 mm. Fig. 1 shows the model of the upward two-phase annular film MHD flow in a cylindrical coordinate system. The polar angle, θ, is measured in counter clockwise direction from x-axis and the axial coordinate, z, is positive out of the paper.

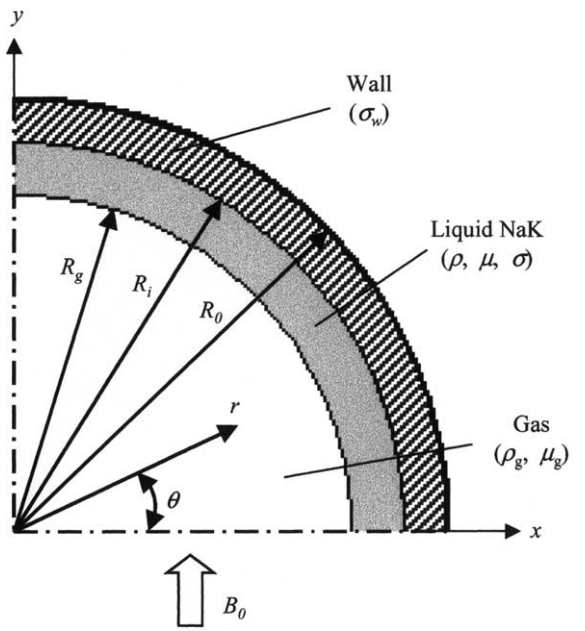

Fig. 1. Cross-section of the fluid in an annular flow and coordinate system.

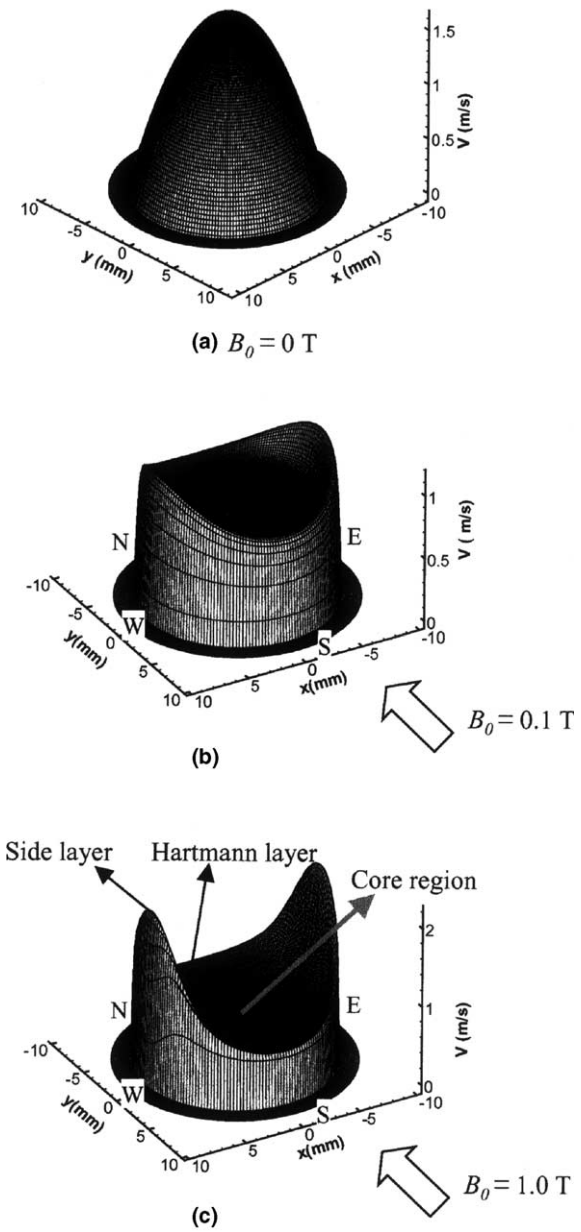

Fig. 2. Velocity profiles of MHD liquid metal flows in a vertical pipe ($Re = 5.3 \times 10^3$).

The principal purpose of the present study was to investigate the flow structures in the liquid film of an annular flow in the presence of a magnetic field. Therefore, a uniform thickness of the liquid film and a non-deformable interface were assumed for simplicity, i.e., no waves exist on the gas–liquid interface and no droplets exist in the gas core. Additionally, the flow was assumed to be fully developed in the simulation, while at the measurement station in experiment, the flow might not yet be under fully developed condition due to the MHD effect.

The governing equations are the conservation of mass, momentum, energy and the interaction of the flow with the magnetic field. Assumptions for simplicity of the analysis are listed below:

- The viscous dissipation and Joule heating are neglected in the energy equation.
- The interaction of the induced magnetic field with the flow is negligible compared with the interaction of the applied magnetic field with the flow.
- The flows are fully developed both hydrodynamically and thermally, and two-dimensional in a cylindrical coordinate system.
- Density, viscosity, specific heat and thermal conductivity of liquid and gas and electrical conductivity and permeability of liquid and solid wall are constant.
- The interface of the annular film flow is circular without deformation.

With the assumption of the fully developed flow, the velocity vector can be explicitly expressed by $V = [0, 0, V_z(r, \theta)]$, where V_z is the velocity component in the axial direction. Thus, the governing equation for mass is automatically satisfied. The assumption of uniform and constant magnetic field imposed perpendicular to the pipe axis indicates that the magnetically induced electric potential is only a function of r and θ, i.e., $\phi = \phi(r, \theta)$, and consequently the induced electric current density is expressed by $j = j(r, \theta)$.

With the above assumptions and considerations, the simplified governing equations in a cylindrical coordinate system are deduced as follows:

- Axial momentum equation

$$-\mu\left(\frac{\partial^2 V_z}{\partial r^2}+\frac{1}{r}\frac{\partial V_z}{\partial r}+\frac{1}{r^2}\frac{\partial^2 V_z}{\partial \theta^2}\right) = -\frac{\partial p}{\partial z}+\rho g - j_x B_0. \tag{1}$$

- Energy equation

$$\rho c_p V_z \frac{\partial T}{\partial z} = \lambda\left(\frac{\partial^2 T}{\partial r^2}+\frac{1}{r}\frac{\partial T}{\partial r}+\frac{1}{r^2}\frac{\partial^2 T}{\partial \theta^2}\right). \tag{2}$$

- Electric potential equation

$$\frac{\partial^2 \phi}{\partial r^2}+\frac{1}{r}\frac{\partial \phi}{\partial r}+\frac{1}{r^2}\frac{\partial^2 \phi}{\partial \theta^2} = -B_0\left(\cos\theta\frac{\partial V_z}{\partial r}-\frac{\sin\theta}{r}\frac{\partial V_z}{\partial \theta}\right). \tag{3}$$

- Ohm's law

$$j_x = -\sigma\left(\cos\theta\frac{\partial \phi}{\partial r}-\frac{\sin\theta}{r}\frac{\partial \phi}{\partial \theta}+B_0 V_z\right), \tag{4a}$$

$$j_y = -\sigma\left(\sin\theta\frac{\partial \phi}{\partial r}+\frac{\cos\theta}{r}\frac{\partial \phi}{\partial \theta}\right), \tag{4b}$$

where j_x and j_y are the components of electric current density in the x and y directions, respectively. x and y are the axes of the Cartesian coordinate system converted from the cylindrical coordinate system. The x-axis is perpendicular to the direction of B_0 and the y-axis is parallel to that of B_0. Note that only the electric current component perpendicular to B_0 contributes to the Lorentz force.

The boundary conditions for velocity, temperature and electric potential are given as follows:

- The no slip boundary condition is given for liquid velocity on the wall surface,

$$V_z = 0, \quad \text{at } r = R_\text{i}. \tag{5}$$

- The Blasius equation for turbulent flow in a smooth pipe is chosen for the friction factor at the smooth liquid–gas interface with non-interfacial-deformation,

$$(C_\text{f})_\text{i} = 0.079 Re_\text{g}^{-0.25}, \tag{6}$$

so that,

$$\mu\frac{\partial V_z}{\partial r} = \tau_\text{i} = (C_\text{f})_\text{i}\cdot\frac{1}{2}\rho_\text{g} V_{0\text{g}}^2 = 0.0395\rho_\text{g} V_{0\text{g}}^2 Re_\text{g}^{-0.25}, \quad \text{at } r = R_\text{g}. \tag{7}$$

- Boundary condition of temperature at inner surface of the pipe wall is

$$\left(\frac{\partial T}{\partial r}\right)_\text{wall} = -\frac{q}{\lambda}, \quad \text{at } r = R_\text{i}. \tag{8}$$

In addition to the assumption of non-deformable liquid–gas interface, no evaporation of liquid metal at the surface (mass transfer) is assumed; and in most applications of an annular flow, the liquid film constitutes the main resistance to heat transfer [24], therefore, the adiabatic condition is applied here at liquid–gas interface,

$$\left(\frac{\partial T}{\partial r}\right)_\text{interface} = 0, \quad \text{at } r = R_\text{g}. \tag{9}$$

- Electric insulation condition at outer surface of the pipe and the interface of gas and liquid [25],

$$\frac{\partial \phi}{\partial r} = 0, \quad \text{at } r = R_0, \tag{10}$$

$$\frac{\partial \phi}{\partial r} = 0, \quad \text{at } r = R_g. \tag{11}$$

- Continuity of normal electric current at liquid–wall interface [25],

$$\sigma \left(\frac{\partial \phi}{\partial r} \right)_{\text{liquid}} = \sigma_w \left(\frac{\partial \phi}{\partial r} \right)_{\text{wall}}, \quad \text{at } r = R_i. \tag{12}$$

For liquid–gas annular flow, Eq. (2) can be deduced as,

$$\frac{2}{R_i^2 - R_g^2} \frac{V_z}{V_{zm}} = \frac{\partial^2 \Theta}{\partial r^2} + \frac{1}{r} \frac{\partial \Theta}{\partial r} + \frac{1}{r^2} \frac{\partial^2 \Theta}{\partial \theta^2}, \tag{13}$$

where

$$V_{zm} = \frac{\int_0^{2\pi} \int_{R_g}^{R_i} V_z(r,\theta) r \, dr \, d\theta}{\pi (R_i^2 - R_g^2)}, \tag{14}$$

the dimensionless temperature,

$$\Theta = \frac{T - T_b}{qR_i/\lambda} \tag{15}$$

and the mixed average value of T,

$$T_b = \frac{\int_0^{2\pi} \int_{R_g}^{R_i} V_z(r,\theta) T(r,\theta) r \, dr \, d\theta}{\int_0^{2\pi} \int_{R_g}^{R_i} V_z(r,\theta) r \, dr \, d\theta}. \tag{16}$$

Following the definition of the mixed average value of Θ, the dimensionless bulk temperature $\Theta_b = 0$.

The boundary conditions of Θ becomes,

$$\frac{\partial \Theta}{\partial r} = -\frac{1}{R_i}, \quad \text{at } r = R_i, \tag{17}$$

$$\frac{\partial \Theta}{\partial r} = 0, \quad \text{at } r = R_g. \tag{18}$$

The heat transfer coefficient, h_θ, is defined as,

$$h_\theta = \frac{q}{T_{w\theta} - T_b}, \tag{19}$$

at an angular position of θ on the inner surface of the solid wall.

Finite difference approach was used for numerically solving Eqs. (1), (3) and (13). The dimensional computed field is a circular area with diameter $2R_0$ of 19.05 mm. The mesh system is of 190×200 mesh points (190 equivalent intervals in the radial direction and 200 equivalent divisions in the polar angular direction) for the total calculation area. For the annular flow, the calculation area includes the solid wall, liquid film region with the thickness of 1.5 mm and gas core region with the diameter $2R_g$ of 12.75 mm. The applied uniform magnetic field ranges from 0 to 1.0 T. The Hartmann number, Ha, ranges from 0 to 847.

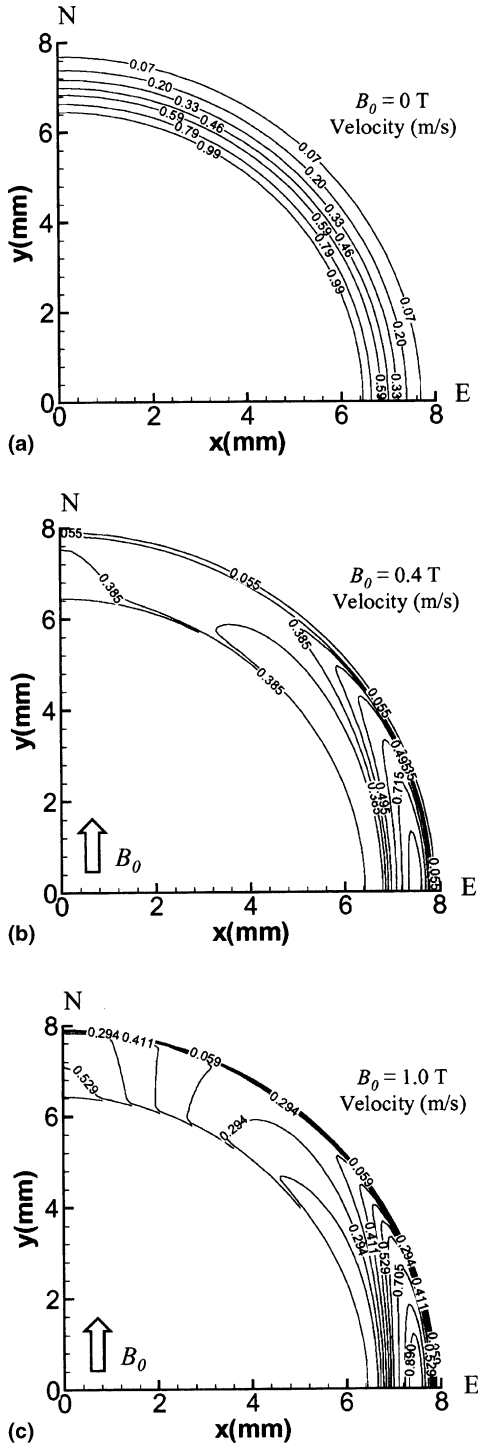

Fig. 3. Development of the asymmetrical velocity distribution in the liquid film of an annular MHD flow ($Re_L = 1.2 \times 10^3$, $Re_g = 1.4 \times 10^4$ and $\delta = 1.5$ mm).

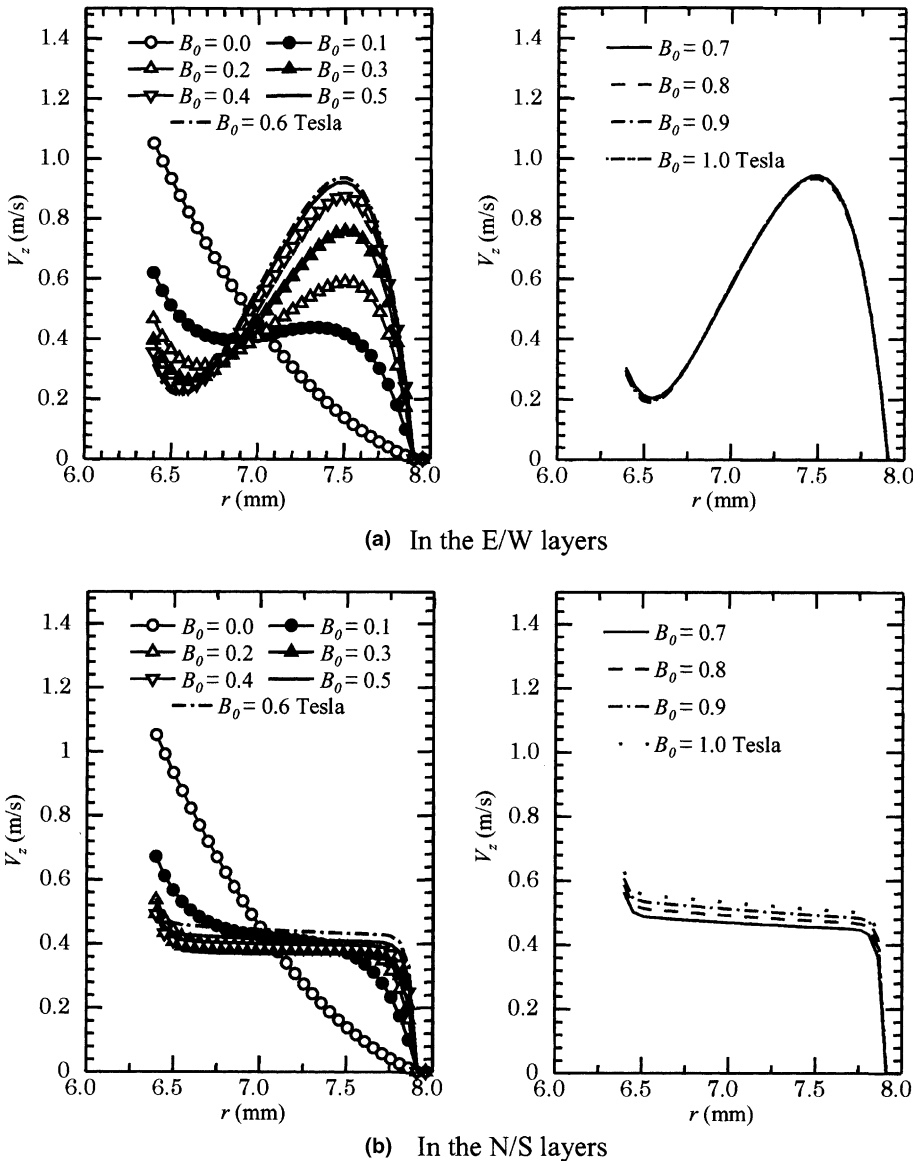

Fig. 4. MHD effect on the velocity distribution in the liquid film of annular flow in a pipe. ($Re_L = 1.2 \times 10^3$, $Re_g = 1.4 \times 10^4$ and $\delta = 1.5$ mm).

3. Verification of program with a single-phase flow

Prior to the analysis of an annular film MHD flow, a single-phase liquid metal MHD flow was simulated for reference in order to verify the computer program and the accuracy. The initial condition of velocity is given by an average velocity for the whole channel cross-section, V_0. In the present analysis, V_0 has been chosen to be fitted to the experimental condition in [16], in order to compare the computational results with the experimental ones. The typical characteristics of flow structures in a liquid metal MHD pipe flow, i.e., evolution of velocity profile with the magnetic field strength and formation of the M-shaped velocity distribution, were obtained, as shown in Fig. 2. Furthermore, the simulated skin friction coefficient showed good agreement with experimental data at similar flow conditions [22]. Owing to the typical velocity distributions in the flow in a transverse magnetic field, an asymmetrical heat transfer rate in the angular direction was obtained: higher on the E/W walls and lower on the N/S walls, which is another typical characteristic of a liquid metal MHD flow [22]. Simulation was then performed for a liquid metal–gas annular MHD flow.

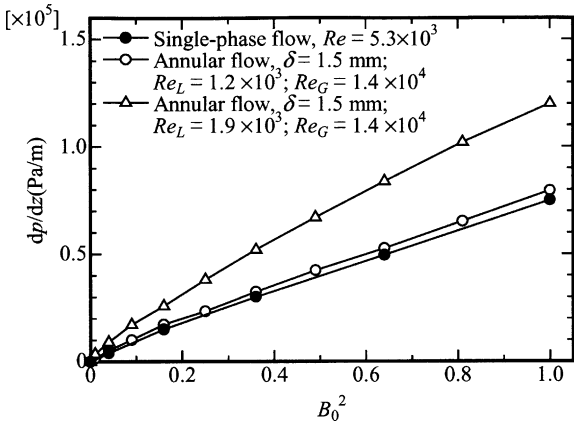

Fig. 5. Pressure drop in a MHD NaK-N_2 annular flow and a single-phase NaK MHD flow.

4. Result

In this section, the predicted velocity distribution and pressure drop, inductive electric current density distribution and heat transfer characteristic are described in order to clarify the mechanism of asymmetric heat transfer in liquid–gas annular MHD flow, from the viewpoint of flow structure in the liquid film.

4.1. Flow structures and pressure drop

The calculated velocity contours in the liquid film of an annular flow for one case are shown in Fig. 3. The side layers in which the velocity is significantly increased are indeed formed in the liquid film near the E/W sidewalls. The side layers become thinner in the direction perpendicular to the magnetic field with increase of the

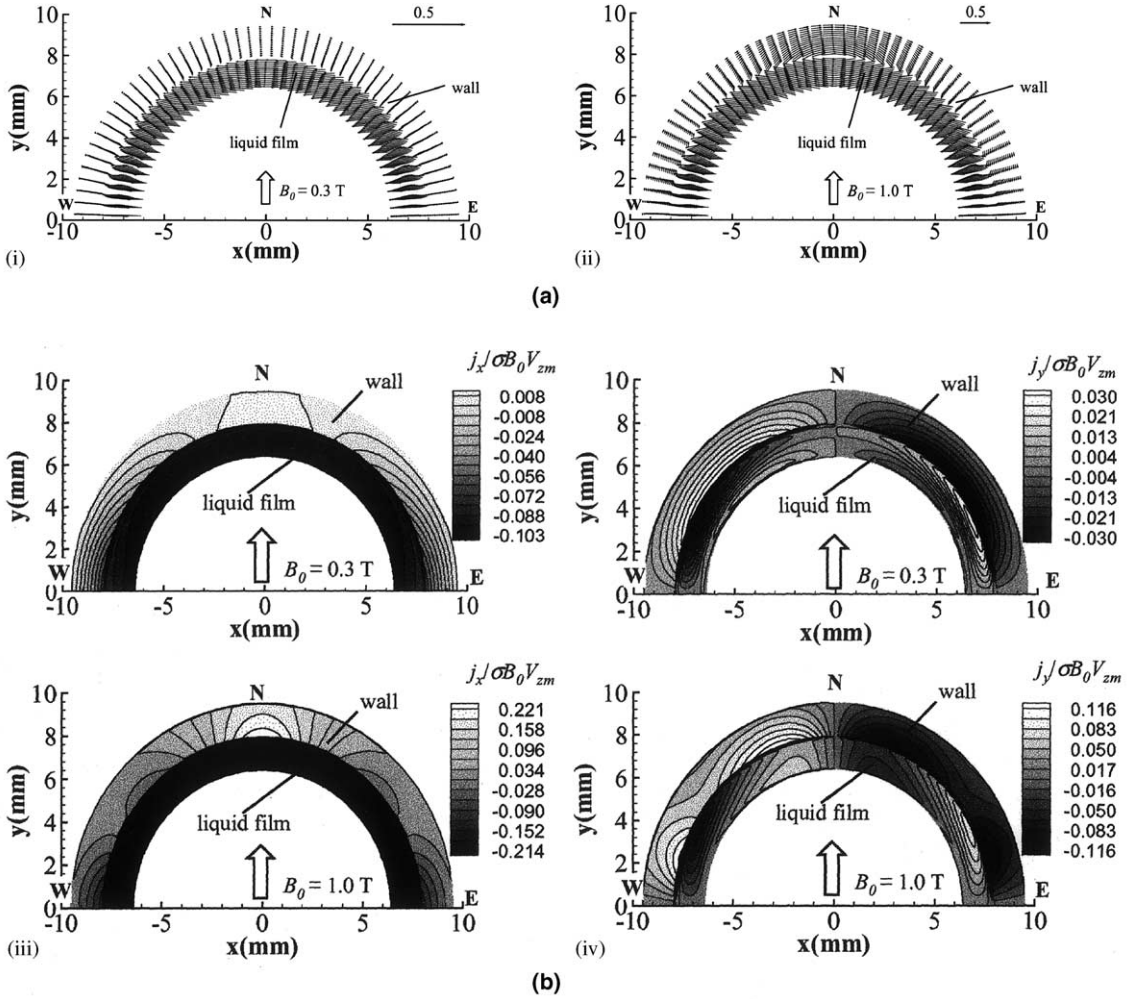

Fig. 6. Dimensionless electric current ($j/\sigma B_0 V_{zm}$) vectors and contour in an annular MHD flow at different B_0($Re_L = 1.2 \times 10^3$, $Re_g = 1.4 \times 10^4$ and $\delta = 1.5$ mm). (a) Dimensionless current density vectors and (b) decomposed dimensionless current contours.

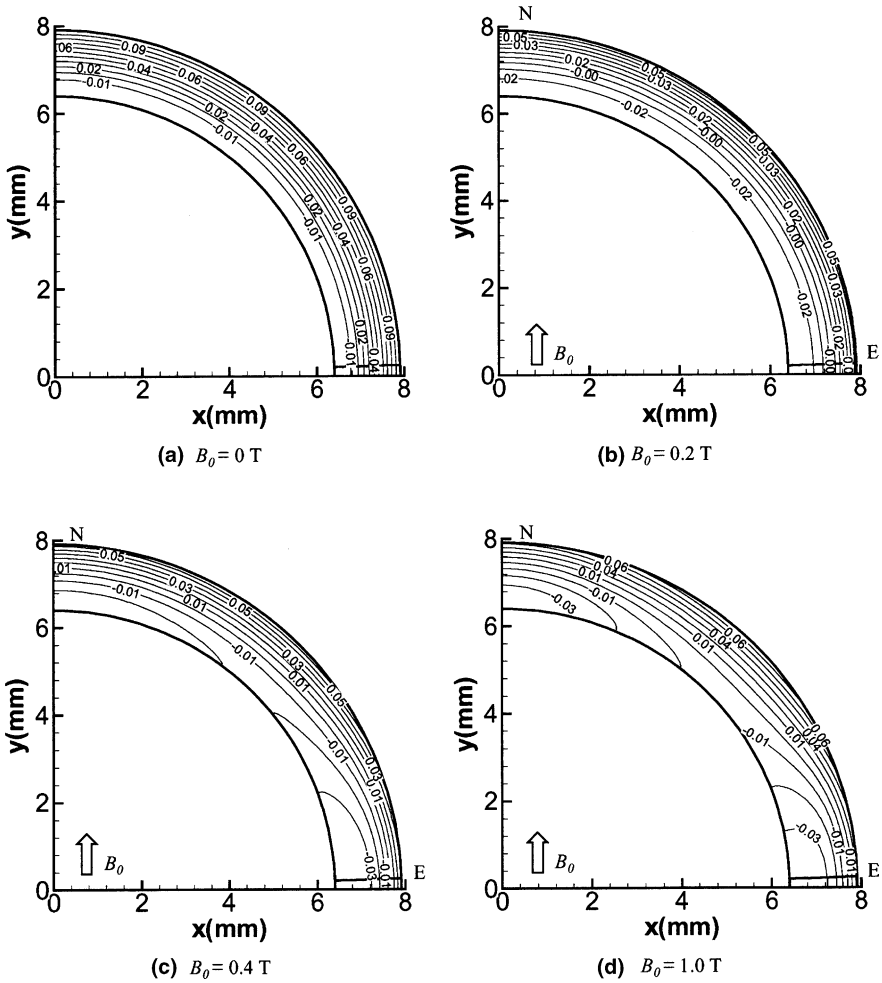

Fig. 7. Dimensionless temperature contours in the liquid film of an annular MHD flow ($Re_L = 1.2 \times 10^3$, $Re_g = 1.4 \times 10^4$ and $\delta = 1.5$ mm).

applied field strength. It is also interesting that the influenced region by the side layers shrinks in the magnetic field direction, or in the angular direction with B_0 (see Fig. 3(b) and (c)).

Fig. 4 shows the MHD effect on velocity distributions in the liquid film near E/W walls and N/S walls respectively. Fig. 4a and b are shown in two parts, left-hand side for cases under field strength up to 0.6 T and right-hand side for cases under field strength from 0.7 T to 1.0 T. It can be seen that the evolution of velocity distribution is evident only when the magnetic field is not so strong ($B_0 < 0.5$ T in this calculation). When the magnetic field is strong enough, that is $B_0 > 0.5$ T, the increase of velocity in the side layers at E/W sidewall regions becomes slower and slower and nearly stops when $B_0 > 0.6$ T (Fig. 4a); and the velocity profile in the whole liquid film at N/S sidewall regions increases slightly with B_0 (Fig. 4b). It implies that the lowest velocity in an annular MHD flow does not always locate in the proximity of the N/S sidewalls but in between N/S and E/W sidewall regions at a strong transverse magnetic field, which is different from a single-phase MHD pipe flow.

Fig. 5 shows the calculated pressure drop of an annular MHD film flow. The simulated pressure drop in a single-phase MHD pipe flow is also plotted for comparison. It is shown that the pressure drop of an annular MHD flow is of the same order in magnitude as that of a single-phase MHD pipe flow with similar average liquid velocity.

4.2. Inductive electric current density field

Fig. 6 illustrates vectors (Fig. 6a) and contours (Fig. 6b) of the dimensionless inductive electric current fields in the liquid film of an annular MHD flow at an applied magnetic field of 0.3 and 1.0 T respectively. Only half of

flow field is shown in the figure since the electric current circuits are formed symmetrically about the x-axis due to the uniform magnetic field and symmetrical flow passage. It is obtained that the electric current flows toward the eastern side in the entire liquid film and return to the western side along circular paths in the electrically conducting wall and in a very thin liquid layer in the near-wall region.

Fig. 6(b) plots the decomposed current density contours in the x and y directions. Note that a comparatively large inductive current component in the direction parallel to B_0 also appears near the N/S sidewalls when the field is strong. This corresponds to the phenomenon that the velocity profiles in the N/S sidewall regions increase with B_0 when B_0 is large and the side layers in E/W regions are much narrowed.

4.3. Heat transfer characteristics

The flow structures straightforwardly influence the heat transfer characteristics. Fig. 7 depicts the evolution of Θ with increase of B_0 in the liquid film of annular flow. In the absence of a magnetic field, the temperature is uniformly distributed in the angular direction. With increase of B_0, the temperature distribution in liquid film becomes more and more asymmetrical. Due to the characteristic velocity distribution as previously described, the temperature contours also display characteristic features when the field strength is large, as shown in Fig. 7(c) and (d). Low temperature spots appear locally near the N/S sidewalls as well as in the E/W sidewall regions at a strong magnetic field.

As a consequence of the non-uniform temperature distribution in the angular direction brought about by the asymmetrical flow structures in the liquid film, the local heat transfer rate at the wall surface is also non-uniform in the angular direction, as shown in Fig. 8. When the applied magnetic field is increased to $B_0 =$ 0.8 T, the minimum value of the Nusselt number is no longer at the N/S sidewalls, which is directly due to the velocity distribution.

Fig. 9 plots the Nusselt number ratio of Nu_{an} for annular flow to Nu_{sn} the for single-phase flow at the E/W and N/S sidewalls with the parameter of field strengths, where only those at the western wall and southern wall are representatively shown in the figure

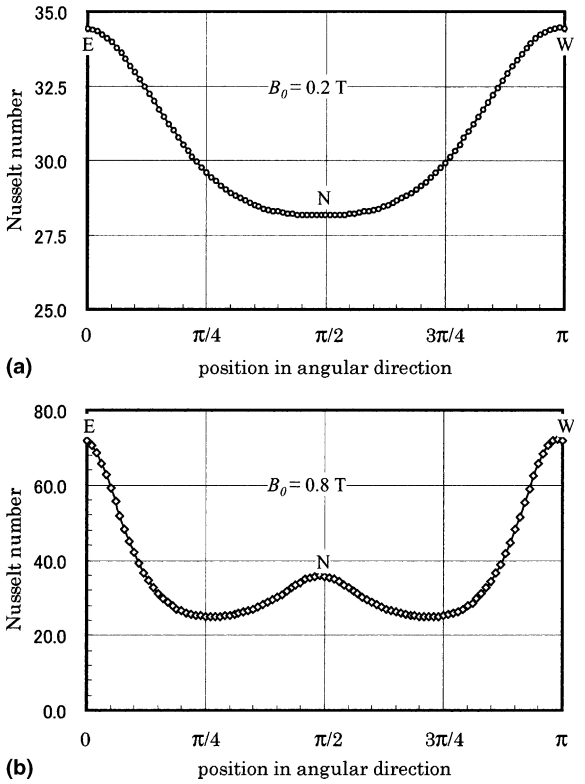

Fig. 8. Local Nusselt number on the wall surface for an annular MHD flow ($Re_L = 1.2 \times 10^3$, $Re_g = 1.4 \times 10^4$ and $\delta = 1.5$ mm). The initial position is at the eastern point of the pipe and measured in counter clockwise direction.

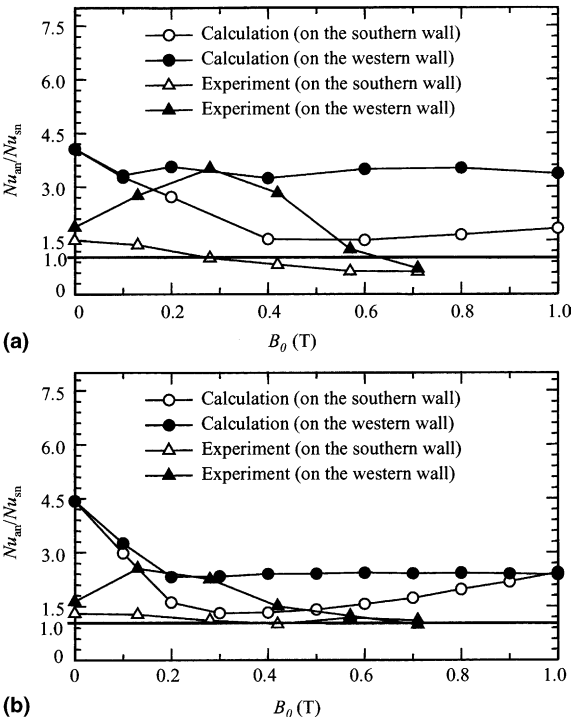

Fig. 9. Asymmetric heat transfer characteristic of annular MHD flow, showing qualitative agreement with experimental results. The Nusselt number of single-phase flow, Nu_{sn}, is for the case of $Re = 5.3 \times 10^3$ in experiment and numerical analysis respectively. (a) $Re_L = 1.2 \times 10^3$, $Re_g = 1.4 \times 10^4$ and $\delta = 1.5$ mm; (b) $Re_L = 1.9 \times 10^3$, $Re_g = 1.4 \times 10^4$ and $\delta = 1.5$ mm.

due to the symmetry of flow passage. The Nusselt number of the single-phase flow, Nu_{sn} is the mean value around the circular tube. The experimental results [16] are also included in the figure for comparison. It is noted here that the Nusselt number does not necessarily shows the minimum value at the southern wall. Nevertheless, the asymmetrical heat transfer characteristic between the surfaces parallel to the direction of the magnetic field and those perpendicular to the field direction has been confirmed numerically. The heat transfer rate on the E/W wall surfaces, designated by solid symbols in the figure, as a whole, is higher than those on the N/S wall surfaces designated by open symbols. This general trend agrees qualitatively with the experimental observations although the predictions are overestimated on both E/W and N/S walls.

The calculated result also shows that the Nusselt number on N/S sidewall surfaces also slightly increases with the applied magnetic field strength from a certain value. This is due to the slight increase of velocity profile near N/S sidewalls at a strong field. Serizawa et al. [16] did not observe such a phenomenon in their experiment, but the Nusselt number kept nearly constant or only slightly decreased with the increase of the magnetic field strength at the same liquid and gas velocity.

5. Summary and conclusions

Numerical simulations were carried out on a liquid metal NaK-nitrogen-gas annular flow in a circular pipe under a transverse magnetic field in order to clarify the flow structures and the characteristics of heat transfer.

The side-layers, in which the liquid flow velocity increased, appeared near the E/W sidewalls. The thickness of side-layers in an annular MHD flow became narrower with increasing the applied field strength not only in the direction perpendicular to the magnetic field but also in the direction parallel to the field.

The appearance of side-layers was due to the distribution of the inducted electric current, i.e., a large current component parallel to the applied field was induced only in a narrow region near the E/W sidewalls. With an increase of the field strength, the distribution of such large current component parallel to the magnetic field might extend angularly to N/S sidewall regions due to the configuration of a circular pipe, so that the side-layer region was shrunk whilst the velocity profile in the N/S sidewall regions had a slight increase.

The temperature field displayed that low temperature spots also locally appeared near the N/S sidewalls as well as in the E/W sidewall layers in a strong magnetic field. In consequence, when the field strength was large, the lowest Nusselt number spot did not locate on the N/S sidewalls any more, which was different from a liquid single-phase MHD pipe flow. The asymmetrical heat transfer behavior between E/W walls and N/S walls qualitatively agreed with experimental observation.

The pressure drop in an annular film MHD flow was of the same order of magnitude as that of a single-phase MHD pipe flow under similar liquid metal flow conditions.

Acknowledgment

We gratefully acknowledge Dr. Y. Kawaguchi, AIST, Japan, for his support and the valuable discussion during the preparation of this paper.

References

[1] J.A. Shercliff, The flow of conducting fluids in circular pipes under transverse magnetic fields, J. Fluid Mech. 1 (1956) 644–666.
[2] R.R. Gold, Magnetohydrodynamic pipe flow. Part 1, J. Fluid Mech. 13 (1962) 505–512.
[3] J.A. Shercliff, Magnetohydrodynamic pipe flow Part 2. High Hartmann number, J. Fluid Mech. 13 (1962) 513–518.
[4] J.C.R. Hunt, Magnetohydrodynamic flow in rectangular ducts, J. Fluid Mech. 21 (1965) 577–590.
[5] J.C.R. Hunt, K. Stewartson, Magnetohydrodynamic flow in a rectangular ducts II, J. Fluid Mech. 23 (1965) 563–581.
[6] C.L. Hwang, K.C. Li, L.T. Fan, Magnetohydrodynamic channel entrance flow with parabolic velocity at the entry, Phys. Fluids 9 (1966) 1134–1140.
[7] E.C. Brouillette, P.S. Lykoudis, Magneto-fluid-mechanic channel flow. I. Experiment, Phys. Fluids 10 (1967) 995–1007.
[8] J.C.R. Hunt, J.A. Shercliff, Magnetohydrodynamics at high Hartmann number, Ann. Rev. Fluid Mech. 3 (1971) 37–62.
[9] C.J.N. Alty, Magnetohydrodynamic duct flow in a uniform transverse magnetic field of arbitrary orientation, J. Fluid Mech. 48 (1971) 429–461.
[10] S. Malang, K. Artheidt, L. Barleon, H.U. Borgstedt, V. Casal, U. Fisher, W. Link, J. Reimann, K. Rust, Self-cooled liquid–metal blanket concept, Fusion Technol. 14 (1988) 1343–1356.
[11] M.A. Abdou, A. Ying, N. Morley, K. Gulec, S. Smolentsev, M. Kotschenreuther, S. Malang, S. Zinkle, T. Rognlien, P. Fogarty, B. Nelson, R. Nygren, K. McCarthy, M.Z. Youssef, N. Ghoniem, D. Sze, C. Wong, M. Sawan, H. Khater, R. Woolley, R. Mattas, R. Moir, S. Sharafat, J. Brooks, A. Hassanein, D. Petti, M. Tillack, M. Ulrickson, T. Uchimoto, The APEX TEAM, On the exploration of innovative concepts for fusion chamber technology, Fusion Eng. Des. 54 (2001) 181–247.
[12] O. Lielausis, Liquid–metal magnetohydrodynamics, Atom. Energy Rev. 13 (1975) 527–581.
[13] I.R. Kirillov, C.B. Reed, L. Barleon, K. Miyazaki, Present understanding of MHD and heat transfer phenomena for liquid metal blanket, Fusion Eng. Des. 27 (1995) 553–569.

[14] N.B. Morley, S. Smolentsev, L. Barleon, I.R. Kirillov, M. Takahashi, Liquid magnetohydrodynamics—recent progress and future directions for fusion, Fusion Eng. Des. 51–52 (2000) 701–713.
[15] J.D. Bender, M.A. Hoffman, A two-phase flow cooling concept for fusion reactor blankets, LLNL Report UCRL—78892, 1977.
[16] A. Serizawa, T. Ida, O. Takahashi, I. Michiyoshi, MHD effect on NaK-nitrogen two-phase flow and heat transfer in a vertical round tube, Int. J. Multiphase Flow 16 (1990) 761–788.
[17] A. Inoue, Y. Kozawa, M. Takahashi, M. Matsuzaki, A. Yoshizawa, Characteristics of flow and heat transfer in air-mercury two-phase stratified flow under a vertical magnetic field, Exp. Therm. Fluid Sci. 8 (1994) 46–57.
[18] M. Takahashi, A. Inoue, M. Aritomi, M. Matsuzaki, Studies on magnetohydrodynamic flow characteristics and heat transfer of liquid metal two-phase flow cooling systems for a magnetically confined fusion reactor, Fusion Eng. Des. 27 (1995) 663–677.
[19] M. Takahashi, N. Umeda, M. Matsuzaki, A. Inoue, M. Aritomi, Heat transfer of lithium single-phase flow and helium–lithium two-phase flow in a circular channel under transverse magnetic field, Fusion Eng. Des. 39–40 (1998) 799–809.
[20] A. Ying, A.A. Gaizer, The effects of imperfect insulator coatings on MHD and heat transfer in rectangular ducts, Fusion Eng. Des. 27 (1995) 634–641.
[21] A. Sterl, Numerical simulation of liquid–metal MHD flows in rectangular ducts, J. Fluid Mech. 216 (1990) 161–191.
[22] F.-C. Li, Falling film and annular flows of liquid metal–gas system with and without magnetic field, Ph.D. thesis, Kyoto University, Japan, 2002.
[23] A. Serizawa, Supplement to "Some asymmetric thermohydrodynamic behaviors of liquid metal–gas two-phase MHD flows" (Invited Lecture), in: Proc. ASME Winter Ann. Meeting, Dollas, USA, HTD-vol. 155, 1990, pp. 331–342.
[24] G.F. Hewitt, N.S. Hall-Taylor, Annular Two-phase Flow, Pergamon Press, 1970.
[25] N. Umeda, M. Takahashi, Numerical analysis for heat transfer enhancement of a lithium flow under a transverse magnetic field, Fusion Eng. Des. 51–52 (2000) 899–907.